Increased crossing of thermal stress thresholds of vegetation under global warming

Xiangyi Li[1]*, Chris Huntingford[2], Kai Wang[1], Jiangpeng Cui[1,3], Hao Xu[1], Fei Kan[1], Hui Yang[1, 4], Josep Peñuelas[5, 6], Shilong Piao[1, 3]*

[1]Institute of Carbon Neutrality, Sino-French Institute for Earth System Science, College of Urban and Environmental Sciences, Peking University, Beijing 100871, China

[2]UK Centre for Ecology and Hydrology, Wallingford, Oxfordshire OX10 8BB, UK

[3]Key Laboratory of Alpine Ecology and Biodiversity, Institute of Tibetan Plateau Research, Center for Excellence in Tibetan Earth Science, Chinese Academy of Sciences, 100085, Beijing China

[4]Department of Biogeochemical Integration, Max Planck Institute for Biogeochemistry, 07745 Jena, Germany

[5]CSIC, Global Ecology Unit CREAF-CSIC-UAB, Bellaterra, Barcelona 08193, Catalonia, Spain

[6]CREAF, Cerdanyola de Vallès, Barcelona 08193, Catalonia, Spain

Affiliations:

[1]Institute of Carbon Neutrality, Sino-French Institute for Earth System Science, College of Urban and Environmental Sciences, Peking University, Beijing 100871, China

[2]UK Centre for Ecology and Hydrology, Wallingford, Oxfordshire OX10 8BB, UK

[3]Key Laboratory of Alpine Ecology and Biodiversity, Institute of Tibetan Plateau Research, Center for Excellence in Tibetan Earth Science, Chinese Academy of Sciences, 100085, Beijing China

[4]Department of Biogeochemical Integration, Max Planck Institute for Biogeochemistry, 07745 Jena, Germany

[5]CSIC, Global Ecology Unit CREAF-CSIC-UAB, Bellaterra, Barcelona 08193, Catalonia, Spain

[6]CREAF, Cerdanyola de Vallès, Barcelona 08193, Catalonia, Spain

*Corresponding author. Email: slpiao@pku.edu.cn, xiangyili@pku.edu.cn

Abstract:

Temperature extremes exert a significant influence on terrestrial ecosystems, but the precise levels at which these extremes trigger adverse shifts in vegetation productivity have remained elusive. In this study, we have derived two critical thresholds, using standard deviations (SDs) of growing-season temperature and satellite-based vegetation productivity as key indicators. Our findings reveal that, on average, vegetation productivity experiences rapid suppression when confronted with temperature anomalies exceeding 1.45 SD above the mean temperature during 2001–2018. Furthermore, at temperatures exceeding 2.98 SD above the mean, we observe the maximum level of suppression, particularly in response to the most extreme high-temperature events. When Earth System Models are driven by a future medium emission scenario, they project that mean temperatures will routinely surpass both of these critical thresholds by approximately the years 2050 and 2070, respectively. However, it is important to note that the timing of these threshold crossings exhibits spatial variation and will appear much earlier in tropical regions. Our finding highlights that restricting global warming to just 1.5°C can increase safe areas for vegetation growth by 13% compared to allowing warming to reach 2°C above preindustrial levels. This mitigation strategy helps avoid exposure to detrimental extreme temperatures that breach these thresholds. Our study underscores the pivotal role of climate mitigation policies in fostering the sustainable development of terrestrial ecosystems in a warming world.

One-Sentence Summary:

This study projects a future norm of exceeding two thermal stress thresholds that suppress vegetation productivity.

Main Text: Temperature extremes are of great concern due to their widespread and profound impacts on human health, the socioeconomic system and ecosystem functioning (*1*, *2*). As the burning of fossil fuel continues, hot extreme events are projected to increase in frequency and intensity (*3*), with unprecedented extreme events already becoming more commonplace (*4*, *5*). Although declining cold extremes under increasing levels of global warming will reduce their damage to future ecosystems (*6*), more frequent expected hot extremes pose a risk of decreasing vegetation productivity and thus suppressing terrestrial carbon uptake (*7*–*9*). Ultimately much more intense temperature anomalies will trigger the failure of land ecosystems (*10*). Yet geographically variable but globally applicable parameters of temperature extremes that define ecosystem suppression have not yet been derived. This lack of understanding hampers determining the emergence time when contemporary extreme temperatures, verified as detrimental to terrestrial ecosystems, will become routine. Filling this knowledge gap to inform policymakers of the global warming levels above which local ecosystem productivity will have a high risk of suffering severe suppression is therefore important.

In this study, we initially established two crucial thresholds for temperature extremes affecting vegetation productivity. This was done through a parallel analysis of growing-season temperature and near-infrared reflectance of terrestrial vegetation data (NIRv) (11). These thresholds signify the points at which major vegetation suppression begins and when ecosystems are fully suppressed. Subsequently, we utilized these thresholds to project various exposure risks for vegetation in the face of temperature extremes under different future global warming scenarios (see Methods). By integrating this information with projections from Earth System Models (ESMs) (12, 13), we estimated locations where future mean temperatures would routinely exceed these thresholds, essentially becoming the new norm (Fig. S1; see Methods). We employed this data to evaluate the effectiveness of the Paris climate targets, aiming for 1.5℃ and 2℃ global mean warming, in mitigating the potential risk posed to land ecosystems by local high growth temperatures. Additionally, we analyzed the compounded impacts of soil moisture (SM) (*14*) deficit during temperature extremes.

Fewer extremes of vegetation than temperatures

The annual growing-season temperature extremes widely exceeded +1 SD (Fig. 1a) or were below -1 SD (Fig. 1b) during the years 2001–2018 (Fig.1a and b). For a normal distribution, in general, it is expected that these thresholds are crossed at an occurrence of ~16%, but our spatial patterns exhibit substantial spatial variability. The conditional probabilities of an extreme NIRv value (i.e., ≤ -1.0 SD) per temperature event revealed that vegetation extremes did not necessarily occur when temperature extremes occurred. The global average conditional probability was 24%, but such probabilities were considerably lower (<15%) for vegetation responses in areas such as southern Australia, Siberia and eastern China (Fig 1c) despite having more frequent high-temperature extremes (Fig. 1a). In contrast, the conditional probabilities were 50-75% in southern North America, Europe, central Asia, southern Australia, eastern Africa and eastern South America, which suggested strongly suppressed vegetation response to high-temperature extremes. Vegetation generally responded more weakly to low-temperature extremes (T ≤ -1.0 SD) (~ 15%), except mainly in some Russian boreal regions (>70% conditional probability, with NIRv ≤-1.0 SD; Fig. 1d).

Extreme temperatures combined with major soil moisture deficits can substantially exceed the negative impacts of separate individual extreme temperature or moisture levels on vegetation productivity (*15*–*18*). We therefore also investigated two types of compound events: hot-dry extremes (T ≥ 1.0 SD and SM ≤ -1.0 SD) and cold-wet extremes (T ≤ -1.0 SD and SM ≥ 1.0 SD)

(Fig. S2). We found that vegetation productivity had a spatially averaged conditional probability exceeding 50% that NIRv ≤ -1.0 SD when hot-dry extremes occurred (Figs. 1 and S2). As expected, such occurrences were mainly in arid and semi-arid regions. Drought and heat stress in these regions were prone to intensify each other through the combination of atmospheric processes and land-atmosphere feedbacks (*16*) so our results showed such circumstances were highly likely to damage vegetation. Regions like the Amazon Basin, however, show a highly frequent occurrence of simultaneous hot-dry extremes but corresponded to low suppressed responses of vegetation productivity. We inferred that available water storage in deep soil in many humid climates, accessible by forests with deep roots, buffered against any water deficit in the upper soil layer, creating strongly resilient ecosystems (*19*). In contrast, compound cold-wet extremes occurred less frequently in most regions (Fig. S2a, b) but often triggered a strong vegetation response in boreal areas (Fig. S2d). Cold extremes combined with wet soils lowered the vegetation demand for water during the growing season so vegetation photosynthesis was strongly limited. Hence the compounded wet extremes combined the damage from simultaneous extremes of frost and waterlogging (*17*, *18*).

Temperature thresholds for vegetation productivity

Our results so far suggest spatially divergent responses of vegetation productivity to temperature extremes, and the additional role of soil moisture in vegetation suppression during temperature extremes. To capture how different levels of temperature extremes trigger detrimental suppressions of vegetation productivity, we next parameterise two intuitive temperature-dependent parameters, χ_1 and χ_2 (schematic, Fig. 2a). The two defining parameters, χ_1 and χ_2, delimit into three phases the probability of suppressed responses of vegetation to increasing temperature extremes at or above different stress levels (*20*). There is a transition at χ_1 from a slow to a rapid rate of change before finally peaking at χ_2 (see Methods). We estimate thresholds for high-temperature extremes without drought impacts (SM > -1.0 SD, χ_{1high} and χ_{2high}) and compounded by drought (SM ≤ -1.0 SD, χ_{1high}^{SM-} and χ_{2high}^{SM-}). Similarly, for low-temperature extremes without high moistures (SM < 1.0 SD, χ_{1low} and χ_{2low}) and with wet extremes (SM ≥ 1.0 SD, χ_{1low}^{SM+} and χ_{2low}^{SM+}) (Fig. 2b-f).

On average and where detected, the onset of the vegetation response to the extremes of high- and low- temperatures occur for χ_{1high} = 1.4 SD and χ_{1low} = -1.7 SD (Fig. 2b, c). Such threshold asymmetry suggests that the impact on vegetation productivity is larger for high-temperature than low-temperature extremes, even for the contemporary climate. We speculate that these impacts may have been due to anthropogenically induced global warming already experienced. We can only detect χ_{1high} in 36% of the global terrestrial surface, mainly at mid- and low latitudes. Threshold χ_{1low} is detected in even much more limited areas, only ~3% of land in some boreal areas (Figs. 2b and S3a). The spatial heterogeneity also suggests that vegetation productivity is much more sensitive to high-temperature extremes in areas such as eastern Australia, northeastern China and parts of Europe and North America because these regions have much lower thresholds (χ_{1high} < 1.0 SD). We cannot determine the value of χ_1 (and especially χ_2) at many locations, because few extreme temperature events of sufficient magnitude occurred during the calibration period 2001–2018 to completely suppress vegetation productivity. Thresholds χ_1 and χ_2 are therefore regarded to be substantial distances from the climatological mean temperature.

The thresholds of maximum vegetation suppression χ_{2high} take an average value of 3.3 SD in the ~15% of the global vegetation surface where data is sufficient to constrain its value (Figs. 2c and S3b). Notable is that χ_{2high} values are markedly lower (<2.0 SD) in northeastern Australia and a small part of southern Africa, so these regions are particularly sensitive to the risk of complete

vegetation failure for relatively low severity of high-temperature extremes. Low-temperature extremes are less likely to cause devastating impacts on vegetation because χ_{2low}, where identified, is <-4.0 SD and detected only in an average of 0.3% of areas.

When considering temperature extremes compounded with soil moisture limitation, this broadens the spatial extents for detectable thresholds and increases the potential damage of temperature extremes in some areas. The geographical coverage of where vegetated areas are detected increased to ~64% for χ_{1high}^{SM-} and ~28% for χ_{2high}^{SM-}, including some Arctic regions (Figs. 2d, e and S3a, b). The additional soil moisture deficit also typically lowers the high-temperature thresholds. Our results indicate that for 57% of the land areas, and mainly at mid- to low latitudes, χ_{1high}^{SM-} is around 1.0 SD detected as being lower than χ_{1high} (Fig. S3c). This finding implies that the suppression impacts of high temperatures and low soil-moisture content combine additively. Such drivers may not, however, be independent. For example, high evaporation is caused by heat stress, so soils dry faster, which reduces water availability and the cooling effects for vegetation (*21*, *22*). We also detect χ_{1low}^{SM+} and χ_{2low}^{SM+} in 2.5- and 10-fold more boreal areas respectively than where χ_{1low} and χ_{2low} are detected. This finding implies that wet extremes cause such vegetation to become much more sensitive to very low-temperature extremes, potentially due to the effect of waterlogging on vegetation productivity (Figs. 1b–d, S3c, d).

Future norm of temperature extremes

Vegetation may be extensively damaged if the adaptive evolution of vegetation fails to keep pace with the rapid rates of warming caused by the human burning of fossil fuel. Vegetation suppression might become much more prevalent if contemporary rare high-temperature events become normal under future climate change. Hence, we used ESMs to determine the year when the decadal-mean temperature of a particular year and the preceding nine years first becomes higher than χ_{1high}- or χ_{2high}-inferred temperatures in Fig. 2. We named these years that become the norm to cross thresholds as the time of emergence of χ_{1high} or χ_{2high} temperature thresholds (abbreviated to the Emergent time, EMt, of χ_{1high} or χ_{2high}) (Figs. 3 and S4). The ESMs we used to derived EMt values are from the Coupled Model Intercomparison Project phase 6 (CMIP6) ensemble and in configurations corresponding to two future scenarios of atmospheric greenhouse gas concentrations, SSP2-4.5 and SSP5-8.5 (Methods).

Where thresholds have been identified, we find that the EMt of χ_{1high} will appear, on average, in the year 2045 under SSP2-4.5 and five years earlier under SSP5-8.5 (Fig. 3a, b). By 2050, 81% (SSP2-4.5) and 89% (SSP5-8.5) of areas will reach or pass the EMt of χ_{1high}. The average EMt of χ_{2high} is predicted to appear after 2072 (SSP2-4.5) and 2060 (SSP5-8.5) (Fig. 3c, d). Higher emissions (i.e. SSP5-8.5), as expected, will accelerate extremes as the future norms, and so >95% of areas where χ_{2high} is detected will have reached the EMt of that threshold by 2080. Some areas, especially tropical areas, are notably likely to attain the EMt of χ_{1high}, and even the EMt of χ_{2high}, in the next one or two decades, providing a major near-term challenge to the resilience of vegetation (Figs. 3a-d and S5). The EMt of χ_{1high}^{SM-} for tropical areas is expected to appear very soon, corresponding to the years of large water deficits, happening 2–3 years before the EMt of χ_{1high} (Fig. 3e, f). Such normalisation of current extremes will occur for almost all tropical areas (~90%) by 2050 although generally later (i.e. after 2050) in many extratropical areas (Fig. S6). These findings illustrate that vegetation suppression may become much more routine for many locations, especially during years of raised water limitation and should the world follow higher future greenhouse gases (GHG) emissions, this will advance the EMt of χ_{1high} and χ_{2high}.

Much of the policy for mitigating climate change is based on determining pathways that decrease fossil-fuel emissions sufficiently to stabilize mean global warming at (or below) either 1.5 or 2 ℃ above pre-industrial levels (*23–24*). With such an emphasis on these warming targets, we thus identified dates of the future norms of local χ_1 and χ_2-inferred temperatures for global mean warming of 1.5 and 2 °C (see Methods). We defined the years in the SSP2-4.5 and SSP5-8.5 scenarios at which global warming crosses 1.5 and 2.0 ℃, and named these as $t_{1.5}$ and $t_{2.0}$, respectively. We find that χ_{1high}-inferred temperatures may become regularly exceeded in ~8% (SSP2-4.5) and ~11% (SSP5-8.5) of global lands, even for levels of global warming constrained to 1.5 ℃ (Figs. 4a and S7a). Areas with EMt $\leq t_{2.0}$ (compared to EMt $\leq t_{1.5}$) will increase by 14% under the 2 ℃ warming of SSP2-4.5. These results also suggest, as expected, that EMt of χ_{1high} will come later if we approach 1.5^{o}C of maximum global warming more slowly (SSP2-4.5 vs SSP5-8.5). Of key importance is that crossing the temperature of the more critical χ_{2high} will continue to be extremely rare for global warming of 2.0 ℃ or below under both two scenarios in almost all locations (Figs. 4b and S7b).

Even policies that strongly mitigate climate change, however, may not be able to prevent the start of at least some suppression of vegetation productivity in locations where there is soil moisture drying in a warming world (Figs. 4c and S7c). For the simulated globally increasing temperatures, our results indicate that the conditional risk of soil-moisture deficits will increase the chances of crossing the $\chi 1_{high}$-inferred temperatures earlier (i.e. EMt of $\chi 1_{high}^{SM-}$ < EMt of $\chi 1_{high}$) and so occurring more before global warming has exceeded either 1.5℃ or 2.0℃, such as in Europe, southern USA, the Amazon Basin, western and eastern Africa, western and eastern Australia, eastern China, India, and parts of Russia. In these regions, hot and dry events are projected to co-occur more frequently and severely, supported by many independent pieces of evidence (*15*, *16*, *25–27*). However, areas remain extremely limited that might cross χ_{2high}^{SM-} routinely in a 1.5 or 2 ℃ world (Figs. 4d and S7d).

For comparison, we also estimated the model-derived temperature thresholds for ESM-based projections of gross primary production (GPP) directly and for simulated years 2001-2018. We found GPP patterns similar to those of the satellite-based thresholds for NIRv (Figs. S8 and S9). The use of GPP also allowed an estimate of the risks of exposure of global land vegetation productivity to the future norms of both χ_{1high}- and χ_{2high}-inferred temperatures based on ESMs (Figs. 4e, f, see also S7e, f and S10). We found that constraining global warming to 1.5 ℃ rather than 2 ℃ will avoid much of the additional potential exposure of GPP to the future norm of extreme high temperatures (Fig. 4e, f). When controlling global warming to 1.5 ℃ under SSP2-4.5, ~2.0×10^7 km^2 of vegetated land will routinely cross the χ_{1high}-inferred temperature. This regular passing of χ_{1high} can start to impact what is ~24.3 PgC/y of GPP in the 1.5 ℃ warming world. The total exposed magnitudes are such that initial suppression could start to affect 75% of the averaged total growing-season GPP during the time period of 2 ℃ warming level, yet much lower at 22% in a 1.5 ℃ world. The exposed vegetated areas and risk to GPP will become even larger with the impact of high soil-moisture deficits (Fig. 4e).

Our analysis of ESMs suggests that the potential impacts on GPP fluxes would be much higher in the tropics. This difference is because more lush tropical vegetation would be affected by the future norm of crossing the χ_{1high}-inferred temperature, even though the vegetated areas affected would be similar between the tropical and temperate regions. Hence, the concern is although rainforests may have a relatively low response to temperature extremes (Fig. 1, 4e and f), due to the very high magnitudes of tropical GPP, any crossing of such thresholds will have a disproportional impact on land-atmosphere CO_2 exchange. We note that some studies report that the tropics are already

showing evidence of becoming destabilizing, indicated by incomplete recovery after extreme events, forest dieback and ongoing loss of resilience (*28–32*). Many ESMs also project the routine occurrence of high-temperature extremes in cold regions including the Arctic, although no such thresholds were identified in the satellite NIRv data (Figs. 2 and S9-11). We suggest that such biases may have been partly associated with the poor representation in the models of vegetation capacity (e.g., adaptation and acclimation) to withstand temperature extremes. Therefore, ESMs tend to underestimate numerical values of thresholds in colder regions when comparing against their equivalent derived from satellite data. Such threshold underestimation will therefore cause ESMs to overestimate the impacts on vegetation productivity when warming levels cause contemporary extremes to become routine (Figs. 2 and S8).

Conclusion

We have identified two temperature extreme thresholds that trigger shifts in land ecosystem productivity and maximize temperature-related damage. Our analysis combines historical temperature records with satellite-based vegetation measurements, revealing spatial variations in these thresholds. Notably, lower temperature thresholds have been identified in eastern Australia, northeastern China, and specific parts of Europe and North America. Additionally, these thresholds decrease further in the presence of conditional soil moisture deficits, indicating additional negative impacts from concurrent droughts on vegetation.

When integrated with Earth System Model (ESM) projections, our study anticipates significant exposure of vegetation productivity to high-temperature extremes. These extremes, currently considered exceptional, are projected to become the norm. Even if global warming is limited to a 2°C increase above preindustrial levels, more than a tenth of Earth's land cover will regularly experience growing-season temperatures exceeding these key thresholds. This scenario highlights the challenge that future warming poses to the current global CO_2 sink, bringing us closer to potential tipping points in terrestrial ecosystems.The suppression of vegetation productivity under a climate with more extreme high temperatures raises concerns about the sustainability of the contemporary terrestrial carbon sink, which offsets CO_2 emissions, in the future (33, 34). Ultimately, our data-derived thresholds represent a substantial advancement in accurately assessing changes in vegetation productivity resulting from temperature extremes. These benchmarks are valuable for calibrating and testing ecological sub-models within ESMs, enhancing the reliability of projections regarding the future evolution of the global carbon cycle.

References

1. von Buttlar, J. et al. Impacts of droughts and extreme-temperature events on gross primary production and ecosystem respiration: a systematic assessment across ecosystems and climate zones. *Biogeosciences* **15**, 1293–1318 (2018).
2. Bastos, A. et al. Direct and seasonal legacy effects of the 2018 heat wave and drought on European ecosystem productivity. *Sci. Adv.* 6, eaba2724 (2020).
3. IPCC Climate change 2021: The physical science basis. Contribution of working group I to the sixth assessment report of the intergovernmental panel on climate change. Cambridge, UK: Cambridge University Press. (2021)
4. Fischer, E. M., Sippel, S. & Knutti, R. Increasing probability of record-shattering climate extremes. *Nat. Clim. Chang.* **11**, 689–695 (2021).

5. Bartusek, S., Kornhuber, K. & Ting, M. 2021 North American heatwave amplified by climate change-driven nonlinear interactions. *Nat. Clim. Chang.* 12, 1143–1150 (2022).

6. Fischer, E. M., Beyerle, U. & Knutti, R. Robust spatially aggregated projections of climate extremes. *Nat. Clim. Chang* **3**, 1033–1038 (2013).

7. Wehrli, K., Hauser, M. & Seneviratne, S. I. Storylines of the 2018 Northern Hemisphere heatwave at pre-industrial and higher global warming levels. *Earth Syst. Dynam.* **11**, 855–873 (2020).

8. King, A. D., Karoly, D. J. & Henley, B. J. Australian climate extremes at 1.5 °C and 2 °C of global warming. *Nat. Clim. Chang* **7**, 412–416 (2017).

9. Zscheischler, J. et al. A typology of compound weather and climate events. *Nat Rev Earth Environ* 1, 333–347 (2020).

10. Reyer, C. P. O. et al. Forest resilience and tipping points at different spatio-temporal scales: approaches and challenges. *J Ecol.* 103, 5–15 (2015).

11. Badgley, G., Field, C. B. & Berry, J. A. Canopy near-infrared reflectance and terrestrial photosynthesis. *Sci. Adv.* 3, e1602244 (2017).

12. O'Neill, B. C. et al. The Scenario Model Intercomparison Project (ScenarioMIP) for CMIP6. Geosci. Model Dev. 9, 3461–3482 (2016).

13. Meinshausen, M. et al. The shared socio-economic pathway (SSP) greenhouse gas concentrations and their extensions to 2500. Geosci. Model Dev. 13, 3571–3605 (2020).

14. Muñoz-Sabater, J. et al. ERA5-Land: a state-of-the-art global reanalysis dataset for land applications. Earth Syst. Sci. Data 13, 4349–4383 (2021).

15. Zhou, S., Zhang, Y., Park Williams, A. & Gentine, P. Projected increases in intensity, frequency, and terrestrial carbon costs of compound drought and aridity events. Sci. Adv. 5, eaau5740 (2019).

16. Alizadeh, M. R. et al. A century of observations reveals increasing likelihood of continental-scale compound dry-hot extremes. Sci. Adv. 6, eaaz4571 (2020).

17. Zohner, C. M. et al. Late-spring frost risk between 1959 and 2017 decreased in North America but increased in Europe and Asia. Proc. Natl. Acad. Sci. U.S.A. 117, 12192–12200 (2020).

18. Yang, H. et al. The detection and attribution of extreme reductions in vegetation growth across the global land surface. Global Change Biology gcb.16595 (2023) doi:10.1111/gcb.16595.

19. Bennett, A. C. et al. Resistance of African tropical forests to an extreme climate anomaly. Proc. Natl. Acad. Sci. U.S.A. 118, e2003169118 (2021).

20. Li, X. et al. Global variations in critical drought thresholds that impact vegetation. National Science Review 10, nwad049 (2023).

21. Zscheischler, J. & Seneviratne, S. I. Dependence of drivers affects risks associated with compound events. *Sci. Adv.* 3, e1700263 (2017).

22. Bevacqua, E., Zappa, G., Lehner, F. & Zscheischler, J. Precipitation trends determine future occurrences of compound hot–dry events. *Nat. Clim. Chang.* 12, 350–355 (2022).

23. King, A. D. Attributing Changing Rates of Temperature Record Breaking to Anthropogenic Influences: CLIMATE CHANGE AND RECORD BREAKING. Earth's Future 5, 1156–1168 (2017).

24. Aadhar, S. & Mishra, V. On the Projected Decline in Droughts Over South Asia in CMIP6 Multimodel Ensemble. J. Geophys. Res. Atmos. 125, (2020).

25. Ionita, M., Dima, M., Nagavciuc, V., Scholz, P. & Lohmann, G. Past megadroughts in central Europe were longer, more severe and less warm than modern droughts. Commun Earth Environ 2, 61 (2021).

26. McKinnon, K. A., Poppick, A. & Simpson, I. R. Hot extremes have become drier in the United States Southwest. Nat. Clim. Chang. 11, 598–604 (2021).

27. Williams, A. P., Cook, B. I. & Smerdon, J. E. Rapid intensification of the emerging southwestern North American megadrought in 2020–2021. Nat. Clim. Chang. 12, 232–234 (2022).

28. Allen, C. D. et al. A global overview of drought and heat-induced tree mortality reveals emerging climate change risks for forests. Forest Ecology and Management 259, 660–684 (2010).

29. Wigneron, J.-P. et al. Tropical forests did not recover from the strong 2015–2016 El Niño event. Sci. Adv. 6, eaay4603 (2020).

30. Boulton, C. A., Lenton, T. M. & Boers, N. Pronounced loss of Amazon rainforest resilience since the early 2000s. Nat. Clim. Chang. 12, 271–278 (2022).

31. Forzieri, G., Dakos, V., McDowell, N. G., Ramdane, A. & Cescatti, A. Emerging signals of declining forest resilience under climate change. *Nature* (2022) doi:10.1038/s41586-022-04959-9.

32. Yang, H. et al. Climatic and biotic factors influencing regional declines and recovery of tropical forest biomass from the 2015/16 El Niño. *Proc. Natl. Acad. Sci. U.S.A.* 119, e2101388119 (2022).

33. Peñuelas, J. et al. Shifting from a fertilization-dominated to a warming-dominated period. *Nat Ecol Evol* 1, 1438–1445 (2017).

34. Penuelas, J. Decreasing efficiency and slowdown of the increase in terrestrial carbon-sink activity. *One Earth* 6, 591–594 (2023).

Acknowledgments:

Funding: This study was supported by the National Natural Science Foundation of China (41988101).

Author contributions: S. Piao and X. Li designed the research; X. Li performed analysis and created all figures. X. Li and C. Huntingford created the first draft of the paper; and all authors contributed to the interpretation of the results and to the text.

Competing interests: The authors declare no competing interests.

Data and materials availability: MCD43C4 is available at https://lpdaac.usgs.gov/products/mcd43c4v006/; ERA5-Land data is available at

https://cds.climate.copernicus.eu/cdsapp#!/dataset/reanalysis-era5-land-monthly-means?tab=overview; Model simulations of CMIP6 is available at https://pcmdi.llnl.gov/CMIP6/.

Supplementary Materials

Materials and Methods

Supplementary Text

Figs. S1 to S12

Tables S1

Reference (*35*)

Figures

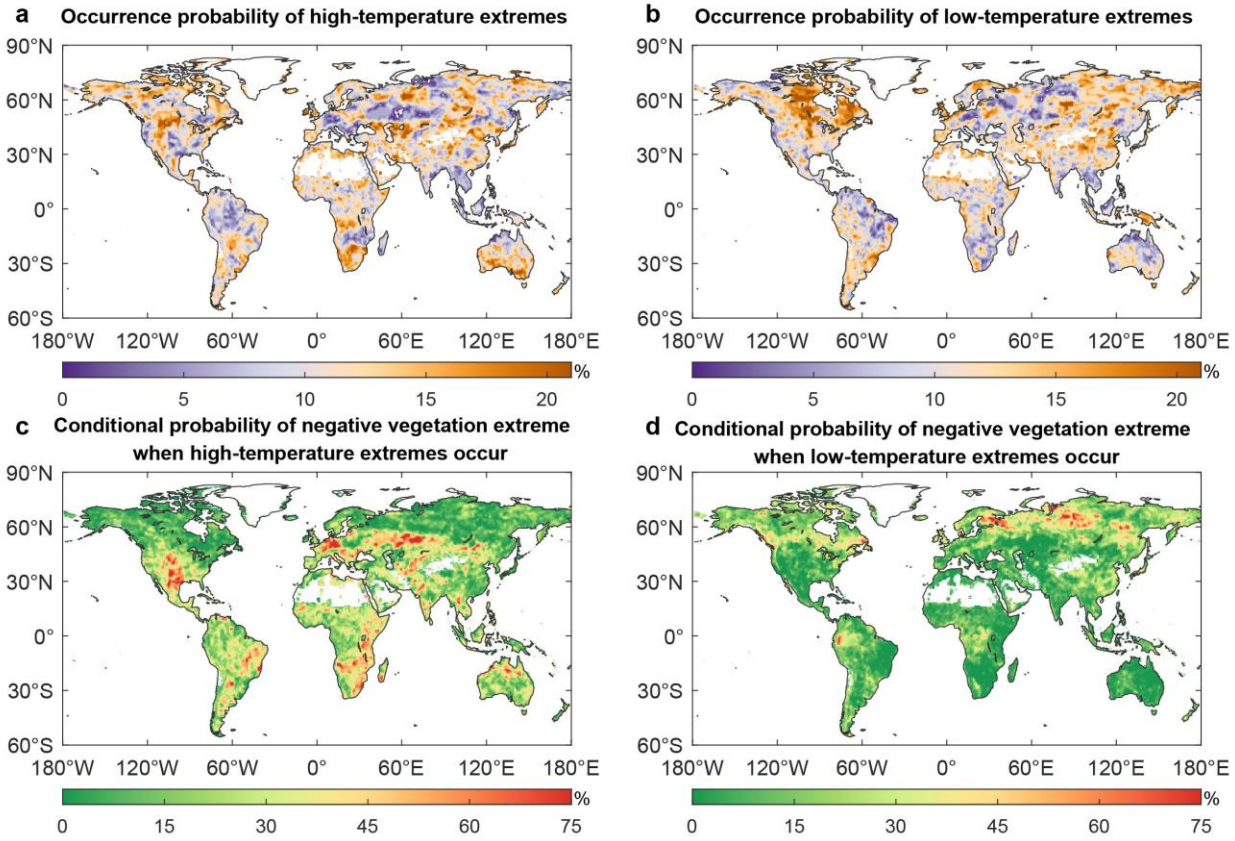

Fig. 1. Temperature extremes and suppressed vegetation response during 2001-2018. a. The probability of occurrence of extreme high temperatures, defined as temperature (T) anomalies ≥1 SD. **b.** The probability of occurrence of extreme low temperatures, defined as temperature (T) anomalies ≤-1 SD. **c.** The conditional probability of the response of vegetation to extreme high temperatures, defined as NIRv anomalies ≤ -1 SD, conditional only on the times when T anomalies are ≥1 SD **d.** The conditional probability of the response of vegetation to extreme low temperatures, defined as NIRv anomalies ≤-1 SD, conditional only on the times when T anomalies are ≤-1 SD. All anomalies correspond to the growing season.

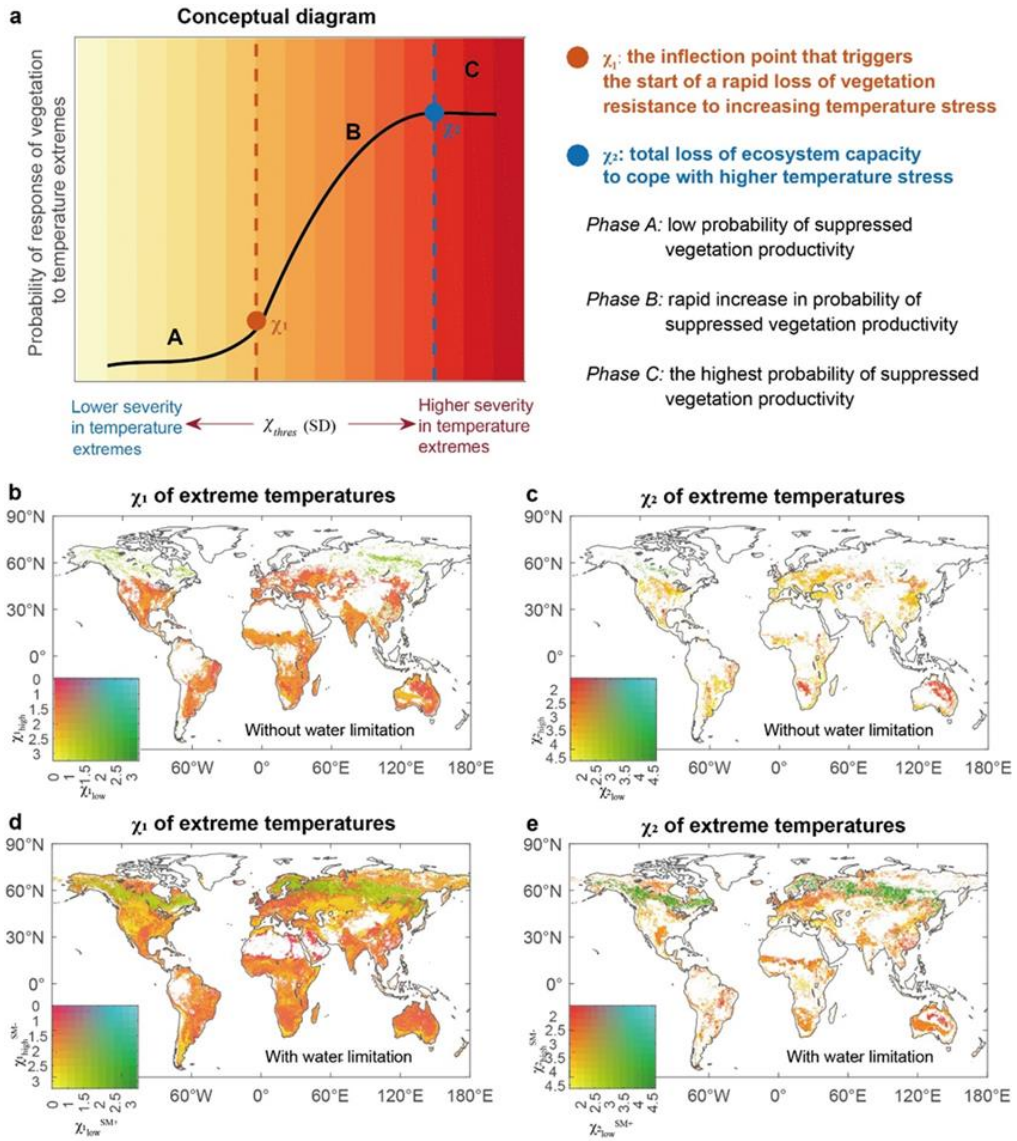

Fig. 2. Temperature thresholds that affect vegetation productivity. a. Conceptual diagram of the probability of the suppression of vegetation productivity with increasing temperature stress, based on the number of standard deviations (SDs) in growing-season temperature from the mean. The curve is derived by considering all years when the absolute values of growing-season temperature anomalies ($|T_{ano}|$) are equal to or larger than any threshold of χ_{thres} on the *x*-axis, i.e. $T_{ano} \geq \chi_{thres}$ for high-temperature extremes and $T_{ano} \leq -\chi_{thres}$ for low-temperature extremes. For each severity level of temperature on the *x*-axis, the probability of vegetation productivity suppressed by 1.0 SD or more during these extreme years is recorded on the *y*-axis. χ_{thres} is measured in units of SD from the local means, and the *y*-axis is measured in units of probability per extreme temperature year. χ_1 and χ_2 are critical temperature thresholds determining the response of vegetation productivity to temperature extremes. Phases A, B and C are the three phases separated by χ_1 and χ_2, as marked (see Methods). **b.** The global pattern of threshold χ_1 of extreme temperature affecting vegetation productivity, derived for all data points except when there is water limitation (SM > -1.0 SD). $\boldsymbol{\chi_{1high}}$: threshold of high temperature, $\boldsymbol{\chi_{1low}}$: threshold for low temperature. **c.** The global pattern of threshold χ_2 of extreme temperature (also SM > -1.0 SD) affecting vegetation productivity. $\boldsymbol{\chi_{2high}}$: threshold of high temperature, $\boldsymbol{\chi_{2low}}$: threshold for low temperature. **d** and **e.** The same as **e** and **f** but for high-temperature extremes compounded with drought ($\boldsymbol{\chi_{1high}}^{\mathbf{SM-}}$ and $\boldsymbol{\chi_{2high}}^{\mathbf{SM-}}$) and low-temperature extremes compounded with wet extremes ($\boldsymbol{\chi_{1low}}^{\mathbf{SM+}}$ and $\boldsymbol{\chi_{2low}}^{\mathbf{SM+}}$). Panels b-e, colour scheme as given by insets. Missing data in panels b-e, shown as white due to insufficient data to constrain χ_1 and χ_2 by observations.

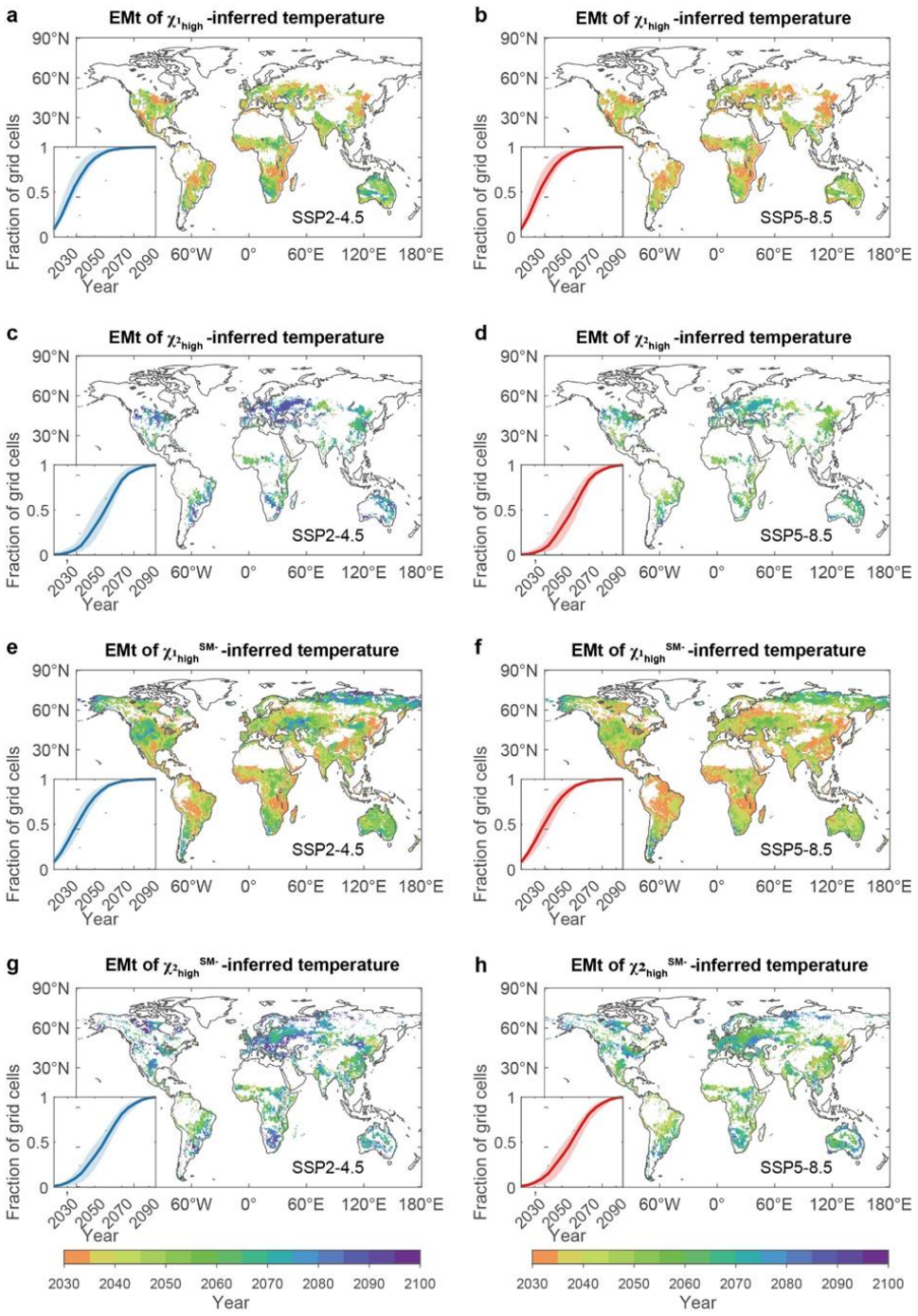

Fig. 3. Times of emergence, EMt, of threshold-inferred high temperature. a. Global pattern of the ESM-average time of the future norm reaching temperature-based thresholds χ_{1high} under SSP2-4.5. The inset shows the cumulative fractions, as a function of time, of normalized grid cells reaching EMt. Calculations are for all grid cells with known values of thresholds χ_{1high}. The shades indicate the ranges of EMt values from different ESMs. **b.** The same as **a** but under the SSP5-8.5 scenario. **c.** The time of the future norm for χ_{2high}-inferred temperature and for the SSP2-4.5 scenario. **d.** The same as **c** but under SSP5-8.5. **e** and **f** The same as **a** and **b** but for χ_{2high}. **g** and **h.** The same as **c** and **d** but for χ_{2high}^{SM-}. Locations in white areas do not necessarily imply that the thresholds will not be crossed during the 21st century, but instead the variability of the contemporary data is insufficient to determine such thresholds. The color bars at the bottom of the figure are common to all panels above them. Panels a, c, e, g (or b, d, f, h) are the emergence times of threshold statistics of Fig. 2 b,c,d,e respectively.

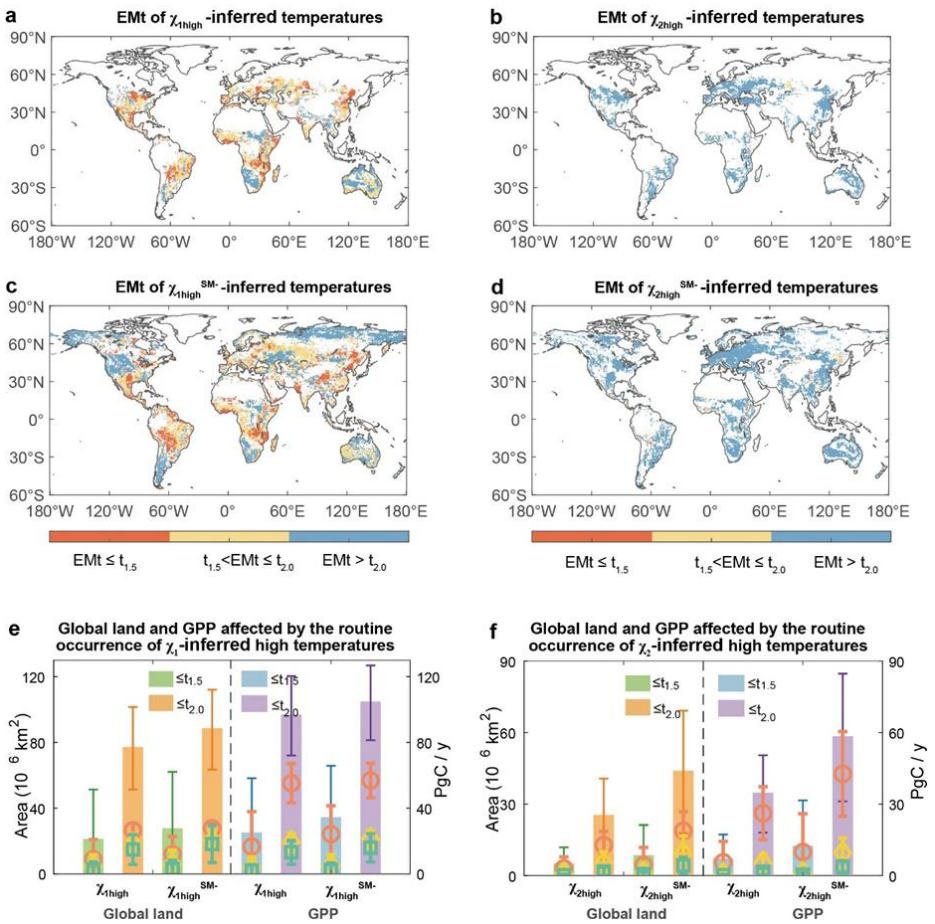

Fig. 4. Times of emergence of the future norms for threshold-inferred high temperatures characterized by whether below 1.5, between 1.5 and 2.0 or above 2.0 °C of global warming in SSP2-4.5 ESM simulations. We are testing if EM$t \leq t_{1.5}$, $t_{1.5}$<EM$t \leq t_{2.0}$ and EM$t > t_{2.0}$. **a** and **b.** For the χ_{1high}- and χ_{2high}-inferred temperatures. **c** and **d.** For the χ_{1high}^{SM-}- and χ_{2high}^{SM-}-inferred temperatures. The colour bars at the bottom of the panels c and d are common to the two panels above them. **e** and **f.** Potential exposure of global land (km^2; left-hand scale) and vegetation productivity (GPP, PgC/y; right-hand scale) to the future norms of (e) χ_{1high}-inferred and (f) χ_{2high}-inferred temperatures at 1.5 °C warming (green for land areas and blue for GPP) and 2 °C warming (orange for land areas and purple for GPP) based on temperature, soil-water content and GPP from the ESMs. The red circles, yellow diamonds and green squares with error bars (indicating the uncertainty among models) represent the contributions from tropical, temperate and cold regions, respectively. The left four bars in each histogram correspond to area (values on the left axes), and the right four bars correspond to GPP (values on the right axes). Each pair of values is divided further based on whether thresholds applied are derived without (χ_{1high} and χ_{2high}) or with drought (χ_{1high}^{SM-} and χ_{2high}^{SM-}) on the *x*-axis.